

PCCP

Accepted Manuscript



This is an *Accepted Manuscript*, which has been through the Royal Society of Chemistry peer review process and has been accepted for publication.

Accepted Manuscripts are published online shortly after acceptance, before technical editing, formatting and proof reading. Using this free service, authors can make their results available to the community, in citable form, before we publish the edited article. We will replace this *Accepted Manuscript* with the edited and formatted *Advance Article* as soon as it is available.

You can find more information about *Accepted Manuscripts* in the [Information for Authors](#).

Please note that technical editing may introduce minor changes to the text and/or graphics, which may alter content. The journal's standard [Terms & Conditions](#) and the [Ethical guidelines](#) still apply. In no event shall the Royal Society of Chemistry be held responsible for any errors or omissions in this *Accepted Manuscript* or any consequences arising from the use of any information it contains.

Mechanics of Graphyne Crumpling

Matthew Becton^a, Liuyang Zhang^a, and Xianqiao Wang^a

^aCollege of Engineering, University of Georgia, Athens, GA 30602 USA

The recent capability of synthesizing large-scale crumpled graphene-related 2D materials has motivated intensive efforts to boost its promising applications in electronics, energy storage, composites and biomedicine. As deformation of graphene-related 2D materials can strongly affect their properties and the performance of graphene-based devices and materials, it is highly desirable to attain subtle control of reversible wrinkling and crumpling of graphene. Graphyne, a 2D lattice of sp^2 - and sp^1 -hybridized carbons similar to graphene, has remained unexplored with respect to its crumpling behavior. Here we employ molecular dynamics simulation to explore the behavior of graphynes under geometric confinement across various temperatures, sizes, and crumpling rates and compare them to graphene under the same conditions, with a focus on the mechanical stabilizing mechanisms and properties of the crumpled structures. The sp^1 -hybridized carbons in graphynes are more potentially reactive than the carbons in graphene; as such the graphynes exhibit a markedly increased affinity for interlayer attraction. It is also shown that the crumpled 2D carbon materials demonstrate a hardness and bulk modulus of an equivalent magnitude with crumpled graphene, with the most important behavior-determining factor being the number of linking sp^1 -hybridized carbons in the material. Our results show that irrespective of initial geometry and crumpling rate, the final structures present intriguing and useful properties which can be incorporated into crumpled graphene structures.

Keywords: Crumpling, Graphyne, Molecular Dynamics, Graphene

1. Introduction

The past decade has seen an explosion of graphene-related research, as this modern age material has demonstrated tremendous potential applications in electronics¹⁻⁴, energy storage^{5, 6}, composites^{7, 8} and biomedicine⁹⁻¹¹ due to its outstanding thermal¹²⁻¹⁴, mechanical¹⁵, and electronic^{16, 17} properties. In these studies and applications, due to its flexible and 2D nature, graphene films are generally wrinkled or rippled with smooth undulations, and/or crumpled with sharp ridges, folds and vertices¹⁸⁻²¹. Many of the useful characteristics of graphene come from its extreme thinness and anisotropic morphology, such that investigations into both this material and those that are similar necessitate a certain focus on the material's associated geometry^{22, 23}. Just as crumpling a piece of paper transforms a sheet-like material into a 3-dimensional object with relatively high compressive strength while maintaining a large surface area and free volume, the same mechanism occurs when crumpling planar nanomaterials such as graphene and its derivatives²⁴⁻²⁶. As the deformation of graphene can strongly affect properties such as diffusion²⁷ and electrical conductivity^{11, 28}, and thus has a notable effect on the performance of graphene-based devices and materials, the potentiality of crumpling as a method to tailor the properties of graphene and graphene oxide while maintaining surface area has been explored in previous works^{26, 29-35}, and it is highly worthwhile to investigate the crumpling behavior of 2D materials similar to graphene as a method of controlled material manufacture.

Graphene is not the only all-carbon 2-D material of interest³⁶; a class of materials called 'graphynes' have been making an impact for their promising properties as well³⁷⁻⁴⁴. Graphynes are a family of 2-D materials composed entirely of carbon similar to graphene; but whereas all of the atoms in graphene are sp^2 -hybridized with three neighbors apiece, graphynes all contain a percentage of sp^1 -hybridized acetylenic linkers, with the percentage and geometry of linkers

defining the type of graphyne^{42, 45, 46}. The inclusion of single and triple bonds and an enlarged lattice gives graphynes markedly different properties when compared with pristine graphene, opening new avenues and giving new alternatives to conventional energy storage⁴⁷, electronics⁴⁸, and filtration technologies^{41, 49, 50}. The graphynes to be used in this work are all γ -graphynes⁵¹⁻⁵⁴, labeled here as N -graphyne where N is the number of acetylenic linkers between hexagonal cells, varied here from 0 to 3 with 0-graphyne referring to graphene. Representative structures of the N -graphynes studies in this work are shown in Figure 1, although it is to be noted that of the structures shown here only 2-graphyne has been achieved synthetically. This work seeks to analyze the crumpling behaviors observed when varying the initial parameters of graphyne composition, system temperature, rate of crumpling, and geometry during the mechanical confinement of graphyne sheets.

2. Computational Methods

Molecular dynamics simulations in this work are based on the open source code LAMMPS⁵⁵. Langevin dynamics and periodic boundary conditions are employed to set up the simulation system. In order to best capture the behavior of the carbon surfaces we utilize the adaptive intermolecular reactive empirical bond order (AIREBO) potential for intra-graphene carbons as described by Stuart et al.⁵⁶ as

$$\mathbf{E} = \frac{1}{2} \sum_i \sum_{j \neq i} \left[\mathbf{E}_{ij}^{REBO} + \mathbf{E}_{ij}^{LJ} + \sum_{k \neq i, j} \sum_{l \neq i, j, k} \mathbf{E}_{kijl}^{TORSION} \right] \quad (1)$$

where the \mathbf{E}_{ij}^{REBO} term is the REBO potential published by Brenner et al.⁵⁷, shown as

$$\mathbf{E}_{ij}^{REBO} = \mathbf{V}_{ij}^R(\mathbf{r}_{ij}) + \mathbf{b}_{ij} \mathbf{V}_{ij}^A(\mathbf{r}_{ij}) \quad (2)$$

where V_{ij}^R is a repulsive term, V_{ij}^A is an attractive term, and b_{ij} is the environmental-dependent bond order term between atoms which activates the attractive term only for bonded atoms. The AIREBO potential is best suited for systems of hydrogen and carbon, rendering the all-carbon system well defined⁵⁶. Since the REBO potential only accounts for interactions of atoms within two Angstroms of one another, the AIREBO potential also includes the E^{LJ} term, which is a standard 12-6 Lennard-Jones potential for distances $2 \text{ \AA} < r < \text{cutoff}$. The cutoff for the LJ term is set here to be 10.2 \AA as a good balance between computation speed and accuracy. The AIREBO potential also includes the $E_{kijl}^{TORSION}$ term, which is a four-body potential describing hydrocarbon dihedral angle preference. The AIREBO potential has previously been used successfully in studying the properties of various graphynes^{49, 53, 58}.

The simulated sample is a single sheet of *N*-graphyne under a Nose-Hoover thermostat with a constant number of atoms and standard velocity-Verlet time integration with timestep of 1fs. The majority of the tested samples are circular sheets with a radius of 10 nm; for the other geometries they are regular polygons with an area equal to the circular sheets. In this work, the initial plane of the nanosheet is considered to be the $x - y$ plane, and perpendicular to the nanosheet is the z direction. Positive z is determined in each sample to be the direction of the first buckling process, as before crumpling both z directions are absolutely symmetric. The boundaries are aperiodic so as to prevent interference in the sample, and a randomized initial velocity is applied to each atom in accordance with the sample temperature with sum zero linear and angular momenta. In order to test crumpling under many conditions, the size, temperature, geometry, and crumpling rate of the samples are varied. The sample is allowed to equilibrate for 400 ps before geometric confinement is applied. The geometric confinement chosen here is spherical, in order to mimic the effect of the aerosol evaporation method of generating crumpled graphene and

graphene oxide^{25, 31, 32, 59}. During geometric confinement a constant normal force is generated spherically around the center of mass of the sample as defined by

$$\mathbf{F}(\mathbf{r}) = -K(\mathbf{r} - \mathbf{R}_c)^2 \quad (3)$$

where K is the force constant equal here to 10 eV/nm^3 , r is the distance from the atom to the center of the confining sphere (which is the same as the center of mass of the graphyne sample), and R_c is the radius of confinement. The confining force is always repulsive and is equal to zero when $r < R_c$. R_c is initially much larger than the sample. As R_c is gradually lessened the sample is forced to crumple to accommodate the reduced volume, as shown in Figure 2. The relative change of R_c with respect to that at the moment of contact with the sample (R_{c0}) will be referred to as ρ_c , defined explicitly as

$$\rho_c = \frac{R_c}{R_{c0}} \quad (4)$$

After the sample has been compressed to a radius 35% that of the original ($\rho_c = 0.35$), the confinement is released and the resulting behavior noted. In the heavy compression test the sample is confined until the number of carbon atoms in the compressed volume is equivalent to the bulk density of graphite (2.267 g/cm^3 or 1.365 u/\AA^3 or $113.75 \text{ carbon atoms/nm}^3$), to ensure that the pressure does not cause amorphous collapse or approach the sp^2/sp^3 hybridization transition⁶⁰.

3. Results and Discussions

3.1. Evolution of the Crumpling Process

To better understand individual processes which contribute to the final behavior of the crumpled graphyne structure, it is useful to take a close look at the evolution of the crumpling process of the nanosheet under spherical confinement. As shown in the graph of Figure 3, the circular

nanosheet sheet is initially flat. As R_c decreases, the 1-graphyne begins to form a “horn” shape, where approximately 50-80% of the sheet buckles in the positive z direction. This bending of the nanosheet strains the C-C bonds, leading to a steady increase in the potential energy of the system, labeled here as U . After this the center “horn” of the nanosheet closes when the two sides are forced together until the two sections of sheet to form van der Waals binding with each other. This is characterized in the graph of Figure 3 by the large drop in U , before a steady increase once again as R_c decreases further. The potential energy of the graphyne undergoes several small drops during the self-adhesion of various sections, but overall there is a steady acceleration in the increase of U . Once R_c has reached the targeted value, the confinement is released and there is a large decrease in U as the pressure is released and the structure seeks an equilibrium state. In more than half of all cases, the overall U in the crumpled state is lower than in the initial planar structure. This phenomenon can be explained by the balance between increased U in the crumples due to a bending of the atomic bonds, and lowered U from the stabilizing effect of interlayer adhesion^{61,62}. Each N -graphyne follows a similar folding pattern, although differences in crumple volume, crumple radius, and collapse speed exist due to the variable stiffness and self-adhesion behaviors between N -graphynes, as discussed in the following section.

Figure 4 shows a potential energy map of the crumpled N -graphynes at the time of confinement release and after the structure has equilibrated. It is notable that 0-graphyne is only held together by edge binding effects at lower temperatures, with interlayer sliding predominating over interlayer adhesion as only the edge carbons are reactive enough at low temperatures to overcome the bending energy imposed by crumpling. The other graphynes show little to no interlayer sliding, and are held together by interlayer van der Waals adhesion effects (with little contribution by edge binding).

The radius of gyration (R_g) is used in this paper as a way to easily describe the approximate size of the crumpled nanosheet structure, defined here as

$$R_g = \sqrt{\frac{1}{n} \sum |r_i^2 - r_{com}^2|} \quad (5)$$

where n is the number of atoms, r_i is the position of the i th atom and r_{com} is the position of the center of mass of the nanosheet. Figure 5 shows the change in U of the N -graphynes versus ρ_g , defined here as the relative change of the radius of gyration of the nanosheet with respect to the initial structure:

$$\rho_g = \frac{R_g}{R_{g0}} \quad (6)$$

After confinement is released the structures partially unfold, visualized in Figure 5 as the potential energy dropping and ρ_g increasing at the end of the run. It is also clear that there is no change in U until the structure begins to change shape, as U and ρ_g begin to change simultaneously and linearly at the beginning of the crumpling process. As is seen in Figure 3 and Figure 5, the final U is often lower than that of the initial structure. This is due to the stabilizing effect of the interlayer adhesion and edge effects on the crumpled structures, making the crumpled structures more energetically favorable and thus more stable.

3.2. Effects of Graphyne Composition

The focus of this study is the crumpling behavior of several varieties of graphyne, and accordingly an important factor in the properties of the final structure is the composition of the initial sample. The integer of acetylenic linkers between hexagonal carbon cells is varied from 0 to 3, with 0-graphyne being graphene as shown in Figure 1. As the unit cell of the 2-D carbon crystal grows larger, the surface density of carbon atoms decreases as depicted in Table 1.

While the behavior of each graphyne is similar during crumpling, the overall bending energy during crumpling is higher for the more dense graphynes, with 0- and 1-graphyne exhibiting very similar behavior. As shown in Figure 5, when U is scaled for the number of atoms the behaviors of 0- and 1-graphyne are extremely close, while the large drop in U of 2- and 3-graphyne relative to the others is caused by a much reduced bending energy as well as a similar per-atom self-adhesion energy. It has been shown previously that as a function of atom density, 1-graphyne is comparable to 0-graphyne in terms of interlayer interaction energy⁴². A close view of the folding process disparities caused by the decreased bending energy/adhesion ratio is presented in Figure 6, where the same stages of crumpling are given for each type of N -graphyne. It is notable that the close-packed crystalline structure and interlayer attraction in graphene allows for increased sliding and gives it a packing behavior similar to an ideal elasto-plastic sheet⁶³, when compared with the graphynes with $N = 1\sim 3$. Another interesting phenomenon is that in the final structures, as seen in part (v) of sections (a), (b), (c), and (d) of Figure 6, the average radius of curvature of the folds in graphene is smaller than 1 nm while in the graphynes it is larger; however the final structure sizes decrease as N goes from 0 to 4.

To estimate the mechanical durability for applications such as lubrication or kinetic energy mitigation, a referential hardness H for each N -graphyne is estimated using the approximation

$H \approx -\frac{dP}{dR_c}$ ²⁶, where P is the pressure, computed as

$$P = \frac{nk_bT}{V} + \frac{\sum_i^N r_i \cdot f_i}{3V} \quad (7)$$

where n is the number of atoms, k_b is Boltzmann's constant, T is the temperature, and f_i is the force felt by the i th atom. The heavy compression runs are used as the basis for this estimation, with the $P - R_c$ graph shown in Figure 7. To estimate H , the 20 ps linear sections at the final

stage of crumpling as seen on the $P - R_c$ curve are utilized. It is interesting to note the initial 'bump' in pressure seen in Figure 7 as compression begins, as this is a good indicator of the inherent stiffness of the material and its initial resistance to bending. Only 0-graphyne and 1-graphyne show a noticeable change in pressure at the start of confinement, revealing the similarity in stiffness between these materials as compared with the higher order graphynes. The bulk modulus of an isotropic material is a measurement of a material's change in volume under uniform pressure, useful to know for high temperature- and pressure-capable materials such as pure carbon structures, which can be used in suitable extreme environments. For the calculation of the hardness and the bulk modulus B , the entire crumpled structure as a whole is considered to be on average an isotropic 3-dimensional structure. While there is a rough correlation between hardness and bulk modulus, unlike hardness, bulk modulus is a material property which is precisely defined; it can be determined by using the formula

$$B = -V \frac{dP}{dV} \quad (8)$$

where V is the volume of the structure. The estimated H and B of each N -graphyne is presented in Table 1, and expectedly these structures have a much lower bulk modulus than that of graphite (≈ 34 GPa), as these structures are not flat layered sheets like graphite, and as such have the flexible ability to respond to environmental stresses without brittle rupture.

Our results indicate that as the number of linkers increases the bending stiffness decreases, thus the apparent interlayer adhesion increases, and the crumpled sample is more likely to be stable upon constraint release. The mechanical properties of 1-graphyne are similar to graphene, as the single triple bond between hexagonal sections is stiff enough to resist bending while still promoting interlayer adhesion. The hardness and bulk modulus of 2- and 3-graphyne are much

lower than those of graphene, as the connecting single bonds are less resistant to bending in addition to the sheer difference in density of the material. These results suggest that as a function of density, 1-graphyne forms quasi-isotropic crumpled structures with hardness and bulk modulus at least on par with crumpled graphene.

3.3. Effects of Graphyne Temperature

A higher temperature generally results in an increase in the flexibility of a material, as a result of excess energy in the atoms and bonds. In accordance with this, results demonstrate a more rigid packing behavior and greater propensity for unfolding upon release at low temperatures; the bonds are less flexible when there is a dearth of kinetic energy in the system. During initial equilibration, a higher amount of kinetic energy causes a larger deviation from the minimized structure, leading to possible asymmetry when the nanosheet encounters the confinement wall. As seen in Figure 8, however, the overall behavior of the crumpling (as characterized by changes in U) does not noticeably change at higher temperatures; there is merely a greater tendency for abnormal crumpling modes to form. The temperature plays a small but definite role in the crumpling behavior of graphynes, and an increased pliability of a material at higher temperatures is to be expected.

3.4. Effects of Crumpling Rate

During material deformation it is important to estimate the dynamic effect on the process⁶⁴⁻⁶⁶, which stems from the speed of deformation and the response rate of the material. In order to ensure that dynamic effects play a small role in our simulation, crumpling is performed at rates of 5, 10, and 50 nm/ns. The crumpling rate refers to the rate of change of the radius of the confining sphere, and here the radius of confinement is always decreasing as the simulation

proceeds. At low crumpling speeds (5, 10 nm/ns) the folding is constantly nearly symmetrical, with circular sections forming the initial ‘horn’ shape and with square sections folding corner-to-corner. The repeatability of the process shows that dynamic effects play a minor role in the evolution of the material deformation. During fast crumpling (50 nm/ns) the initial behavior of the nanosheet is much less deterministic, folding in a more random fashion as dynamic effects shape the initial crumpling modes. Additionally, during fast crumpling there is a near-constant increase in the potential energy of the system until constraint release, as the self-adhesion related drops in U are overwhelmed by the stresses caused by rapid confinement. A comparison of crumpling rates for 1-graphyne is given in Figure 9, where the x -components of the graph are aligned for ease of visual comparison; i.e., the 10, 50, and 500 nm/ns crumpling rate graphs are stretched by magnitudes of 2, 10, and 100 respectively, so that the scales are the same as the 5 nm/ns crumpling rate. It is clear from the increased potential energy change that the nanosheet undergoes higher stress at higher rates of crumpling, and dynamic effects dominate the folding process at 50 and 500 nm/ns as evidenced by the lack of the characteristic large drop in U as the sheet self-adheres.

3.5. Effects of Graphyne Geometry

In determining both the final crumpling state and the process by which the graphyne evolves, it is important to consider the influence caused by the initial shape of the nanosheet. In this study, a circular sample, a square sample, and a triangular sample of equal area are compared under the same conditions and the results are observed. Results show that circular sheets of N -graphyne under symmetric spherical confinement always demonstrate the afore-mentioned ‘horn’ shape, before self-adhering and folding into the “rolled-up” shape. Due to the corners of the structure encountering the confinement before the edges, square sheets tend to fold with a “pouch” shape

where the diagonal corners of the square fold towards one another, with each corner bending towards the same z direction. Corners connect to each other, while the center of the nanosheet buckles in the positive z direction. This structure then undergoes buckling until the sheet self-adheres, finally collapsing into an indeterminately folded sheet. Figure 10 shows the evolution of the square and triangular nanosheets along with comparable stages of the circular nanosheet. The triangular nanosheets fold with a 2:1 corner pattern, in which two corners bend in the same z direction while one bends towards the opposite. This forms a “chair” shape, as shown in Figure 10, before proceeding towards a crumpled final structure quite similar to nanosheets of other geometries, whose properties depend most strongly on N . For both the square and triangular nanosheets, the bulk modulus and hardness were within 10% of that of circular nanosheets of the same composition. In order to determine size effects for this nanometer range, sheets with an area 9 times larger than the initial structures are tested and the folding pattern for each graphyne is very similar to the smaller nanosheets. The formation of the initial “horn” shape is shown in Figure 11, synonymous with stage (i) in Figure 5. Our evidence points towards the conclusion that the particular N -graphyne composition of the nanosheet is more influential in determining the mechanical properties of the final crumpled structure (at the tens of nanometer range) than absolute size or geometry of the nanosheet.

4. Conclusions

In summary, we have performed molecular dynamics simulation to investigate confinement-induced crumpling of nanosheets of N -graphynes. It has been indicated that the number of acetylenic linkers (N) of the graphyne is the strongest indicator of the behavior and mechanical properties of the material. The crumpling process is also influenced by temperature and crumpling rate, with the geometry of the nanosheet playing a large role in the initial crumpling

behavior. By rationally designing a crumpling process, the desired end product can be obtained. It is to be noted, however, that these findings only pertain to pristine graphynes, with no defects or inclusion of species beyond carbon. Defects or reactive species such as oxygen (as in graphene oxide) could promote a more robust final structure due to interlayer bonding, as has been shown before²⁶. These fundamental findings in this paper provide a promising platform for quantitatively transforming 2-D materials into 3-D isotropic nanoparticles with nonconventional properties and also can serve as a guideline to design novel carbon-based nanomaterials and nanodevices.

Acknowledgements

The authors acknowledge support from the University of Georgia (UGA) Research Foundation. Calculations are performed at the UGA Advanced Computing Resource Centre.

Author information

Corresponding author: Xianqiao Wang

Email: xqwang@uga.edu.

Competing financial interests: The authors declare no competing financial interests.

References

1. P. Blake, P. D. Brimicombe and R. R. Nair, *Nano Lett*, 2008, **8**, 1704-1708.
2. V. Yong and J. M. Tour, *Small*, 2010, **6**, 313-318.
3. C. Jeong, P. Nair, M. Khan, M. Lundstrom and M. A. Alam, *Nano Lett*, 2011, **11**, 5020-5025.
4. M. Y. Liao and Y. Koide, *Crit Rev Solid State*, 2011, **36**, 66-101.
5. D. Deng and J. Y. Lee, *Chem Mater*, 2007, **19**, 4198-4204.
6. Y. F. Li, Z. Zhou, P. W. Shen and Z. F. Chen, *Chem Commun*, 2010, **46**, 3672-3674.
7. M. A. Rafiee, J. Rafiee, I. Srivastava, Z. Wang, H. H. Song, Z. Z. Yu and N. Koratkar, *Small*, 2010, **6**, 179-183.
8. D. Konatham, K. N. D. Bui, D. V. Papavassiliou and A. Striolo, *Mol Phys*, 2011, **109**, 97-111.
9. Y. J. Hu, J. A. Jin, H. Zhang, P. Wu and C. X. Cai, *Acta Phys-Chim Sin*, 2010, **26**, 2073-2086.
10. C. A. Merchant, K. Healy, M. Wanunu, V. Ray, N. Peterman, J. Bartel, M. D. Fischbein, K. Venta, Z. T. Luo, A. T. C. Johnson and M. Drndic, *Nano Lett*, 2010, **10**, 2915-2921.
11. R. Kempaiah, A. Chung and V. Maheshwari, *Acs Nano*, 2011, **5**, 6025-6031.
12. S. Subrina and D. Kotchetkov, *J Nanoelectron Optoe*, 2008, **3**, 249-269.
13. V. Varshney, S. S. Patnaik, A. K. Roy, G. Froudakis and B. L. Farmer, *Acs Nano*, 2010, **4**, 1153-1161.
14. A. V. Eletskii, I. M. Iskandarova, A. A. Knizhnik and D. N. Krasikov, *Phys-Usp+*, 2011, **54**, 227-258.
15. A. Sakhaee-Pour, *Comp Mater Sci*, 2009, **45**, 266-270.
16. V. M. Pereira, A. H. C. Neto, H. Y. Liang and L. Mahadevan, *Phys Rev Lett*, 2010, **105**, 156603.
17. O. V. Yazyev and S. G. Louie, *Nature Materials*, 2010, **9**, 806-809.
18. P. Cendula, S. Kiravittaya, I. Monch, J. Schumann and O. G. Schmidt, *Nano Lett*, 2011, **11**, 236-240.
19. S. S. Chen, A. L. Moore, W. W. Cai, J. W. Suk, J. H. An, C. Mishra, C. Amos, C. W. Magnuson, J. Y. Kang, L. Shi and R. S. Ruoff, *Acs Nano*, 2011, **5**, 321-328.
20. D. Fujita, *Sci Technol Adv Mat*, 2011, **12**, 044611.
21. N. Liu, Z. Pan, L. Fu, C. Zhang, B. Dai and Z. Liu, *Nano Res*, 2011, **4**, 996-1004.
22. J. Zhang, J. L. Xiao, X. H. Meng, C. Monroe, Y. G. Huang and J. M. Zuo, *Phys Rev Lett*, 2010, **104**, 166805
23. K. Kim, Z. Lee, B. D. Malone, K. T. Chan, B. Alemán, W. Regan, W. Gannett, M. F. Crommie, M. L. Cohen and A. Zettl, *Phys Rev B*, 2011, **83**, 245433.
24. J. Y. Luo, H. D. Jang, T. Sun, L. Xiao, Z. He, A. P. Katsoulidis, M. G. Kanatzidis, J. M. Gibson and J. X. Huang, *Acs Nano*, 2011, **5**, 8943-8949.
25. F. Guo, M. Creighton, Y. T. Chen, R. Hurt and I. Kulaots, *Carbon*, 2014, **66**, 476-484.
26. C. Chang, Z. G. Song, J. Lin and Z. P. Xu, *Rsc Adv*, 2013, **3**, 2720-2726.
27. S. Jungthawan, P. Reunchan and S. Limpijumnong, *Carbon*, 2013, **54**, 359-364.
28. B. D. Briggs, B. Nagabhirava, G. Rao, R. Geer, H. Y. Gao, Y. Xu and B. Yu, *Appl Phys Lett*, 2010, **97**.
29. W. N. Wang, Y. Jiang and P. Biswas, *J Phys Chem Lett*, 2012, **3**, 3228-3233.
30. S. Mao, Z. H. Wen, H. Kim, G. H. Lu, P. Hurley and J. H. Chen, *Acs Nano*, 2012, **6**, 7505-7513.
31. X. F. Ma, M. R. Zachariah and C. D. Zangmeister, *Nano Lett*, 2012, **12**, 486-489.
32. X. F. Ma, M. R. Zachariah and C. D. Zangmeister, *J Phys Chem C*, 2013, **117**, 3185-3191.
33. O. C. Compton, S. Kim, C. Pierre, J. M. Torkelson and S. T. Nguyen, *Adv Mater*, 2010, **22**, 4759-+.
34. S. W. Cranford and M. J. Buehler, *Phys Rev B*, 2011, **84**, 205451.
35. J. R. Zang, S.; Pugno, N.; Wang, Q.; Tu, Q.; Buehler, M.; Zhao, X., *Nat Mater*, 2013, **12**, 321-325.
36. A. N. Enyashin and A. L. Ivanovskii, *Phys Status Solidi B*, 2011, **248**, 1879-1883.

37. J. H. Zhao, N. Wei, Z. Z. Fan, J. W. Jiang and T. Rabczuk, *Nanotechnology*, 2013, **24**, 095702
38. R. Majidi and A. R. Karami, *Physica E*, 2013, **54**, 177-180.
39. V. R. Coluci, D. S. Galvao and R. H. Baughman, *J Chem Phys*, 2004, **121**, 3228-3237.
40. H. C. Bai, Y. Zhu, W. Y. Qiao and Y. H. Huang, *Rsc Adv*, 2011, **1**, 768-775.
41. Y. Jiao, A. J. Du, M. Hankel, Z. H. Zhu, V. Rudolph and S. C. Smith, *Chem Commun*, 2011, **47**, 11843-11845.
42. S. W. Cranford and M. J. Buehler, *Carbon*, 2011, **49**, 4111-4121.
43. S. W. Cranford and M. J. Buehler, *Nanoscale*, 2012, **4**, 4587-4593.
44. Y. Y. Zhang, Q. X. Pei, C. M. Wang, Y. Cheng and Y. W. Zhang, *J Appl Phys*, 2013, **114**.
45. J. Cao, C. P. Tang and S. J. Xiong, *Physica B-Condensed Matter*, 2012, **407**, 4387-4390.
46. S. W. Cranford, D. B. Brommer and M. J. Buehler, *Nanoscale*, 2012, **4**, 7797-7809.
47. K. Srinivasu and S. K. Ghosh, *J Phys Chem C*, 2012, **116**, 5951-5956.
48. J. Kang, J. B. Li, F. M. Wu, S. S. Li and J. B. Xia, *J Phys Chem C*, 2011, **115**, 20466-20470.
49. J. L. Kou, X. Y. Zhou, H. J. Lu, F. M. Wu and J. T. Fan, *Nanoscale*, 2014, **6**, 1865-1870.
50. C. Q. Zhu, H. Li, X. C. Zeng, E. G. Wang and S. Meng, *Sci Rep-Uk*, 2013, **3**, 3163.
51. M. W. Zhao, W. Z. Dong and A. Z. Wang, *Sci Rep-Uk*, 2013, **3**.
52. M. M. Xue, H. Qiu and W. L. Guo, *Nanotechnology*, 2013, **24**.
53. Y. Y. Zhang, Q. X. Pei and C. M. Wang, *Comp Mater Sci*, 2012, **65**, 406-410.
54. S. Ajori, R. Ansari and M. Mirnezhad, *Mat Sci Eng a-Struct*, 2013, **561**, 34-39.
55. S. Plimpton, *J Comput Phys*, 1995, **117**, 1-19.
56. S. J. Stuart, A. B. Tutein and J. A. Harrison, *J Chem Phys*, 2000, **112**, 6472-6486.
57. D. W. Brenner, O. A. Shenderova, J. A. Harrison, S. J. Stuart, B. Ni and S. B. Sinnott, *J Phys-Condens Mat*, 2002, **14**, 783-802.
58. Y. F. Li, D. Datta, Z. H. Li and V. B. Shenoy, *Comp Mater Sci*, 2014, **83**, 212-216.
59. N. Patra, B. Y. Wang and P. Kral, *Nano Lett*, 2010, **239**, 3766-3771.
60. H. W. Day, *Am Mineral*, 2012, **97**, 52-62.
61. X. H. Meng, M. Li, Z. Kang, X. P. Zhang and J. L. Xiao, *J Phys D Appl Phys*, 2013, **46**, 055308.
62. S. Cranford, D. Sen and M. J. Buehler, *Appl Phys Lett*, 2009, **95**, 123121.
63. T. Tallinen, J. A. Astrom and J. Timonen, *Nature Materials*, 2009, **8**, 25-29.
64. G. P. Zou, Z. L. Chang and Y. J. Qiao, *Chinese Ceramics Communications*, 2010, **105-106**, 75-78.
65. M. Jopek, M. Forejt and J. Buchar, *Metal Forming 2000*, 2000, 729-732.
66. R. W. Armstrong and S. M. Walley, *Int Mater Rev*, 2008, **53**, 105-128.

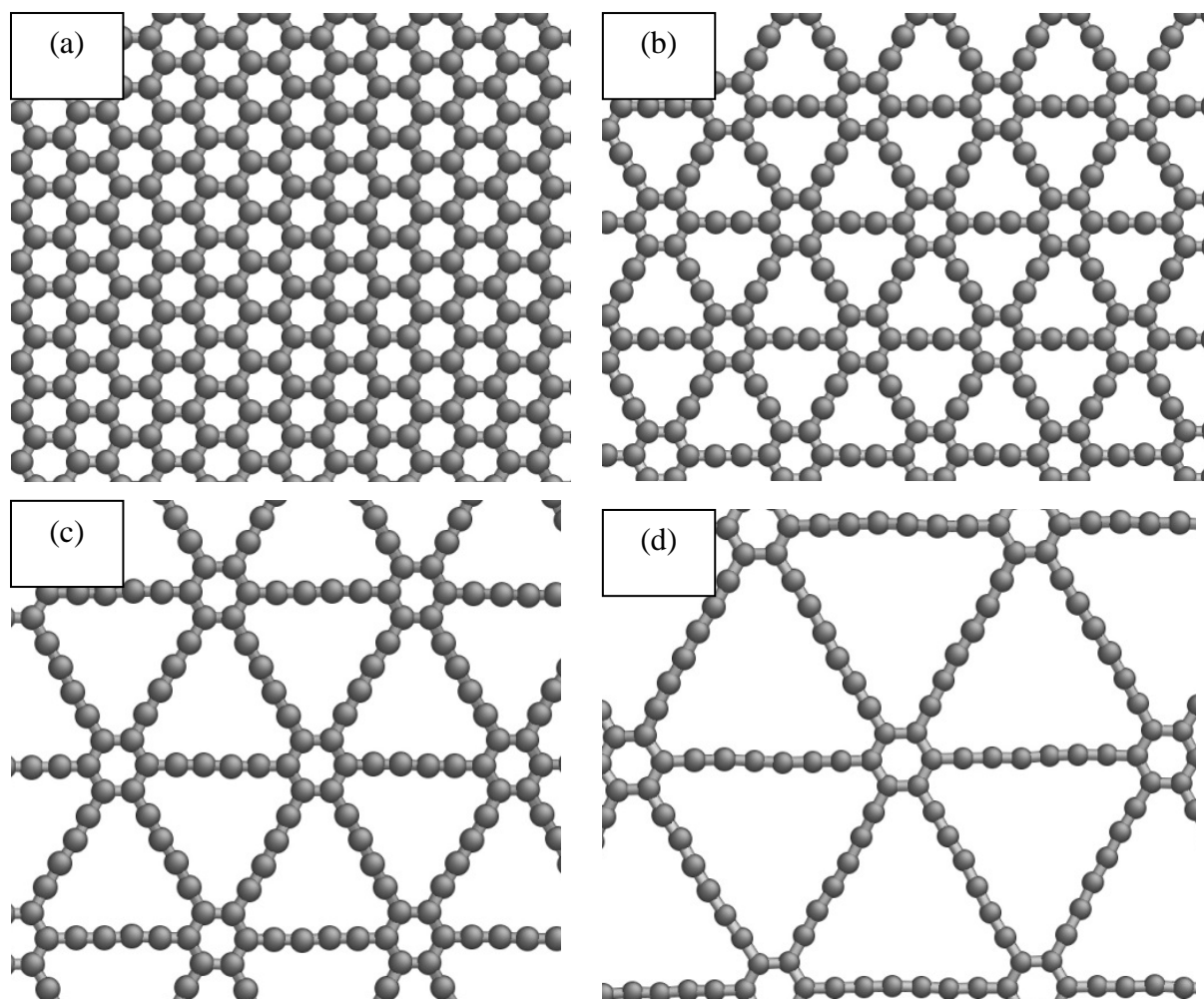


Figure 1: Geometry of materials (a) 0-graphyne [graphene] (b) 1-graphyne [γ -graphyne]

(c) 2-graphyne [graphdiyne] (d) 3-graphyne [graphtriyne]

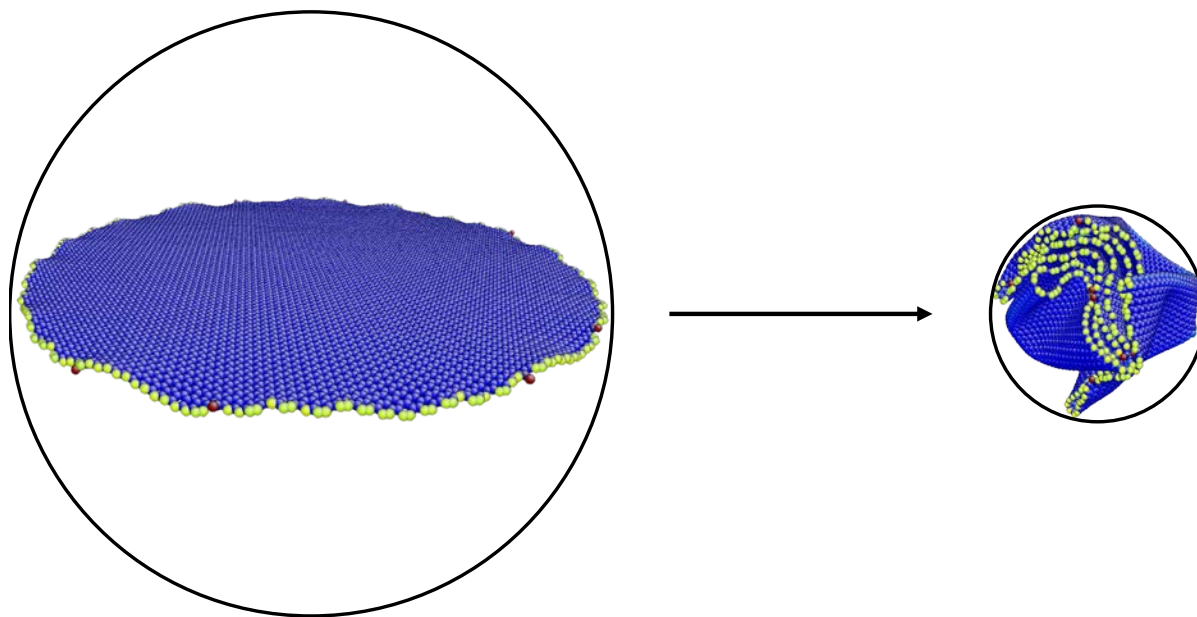


Figure 2: Setup showing 0-graphyne within the confinement boundary as R_c decreases from the initial state to the final state.

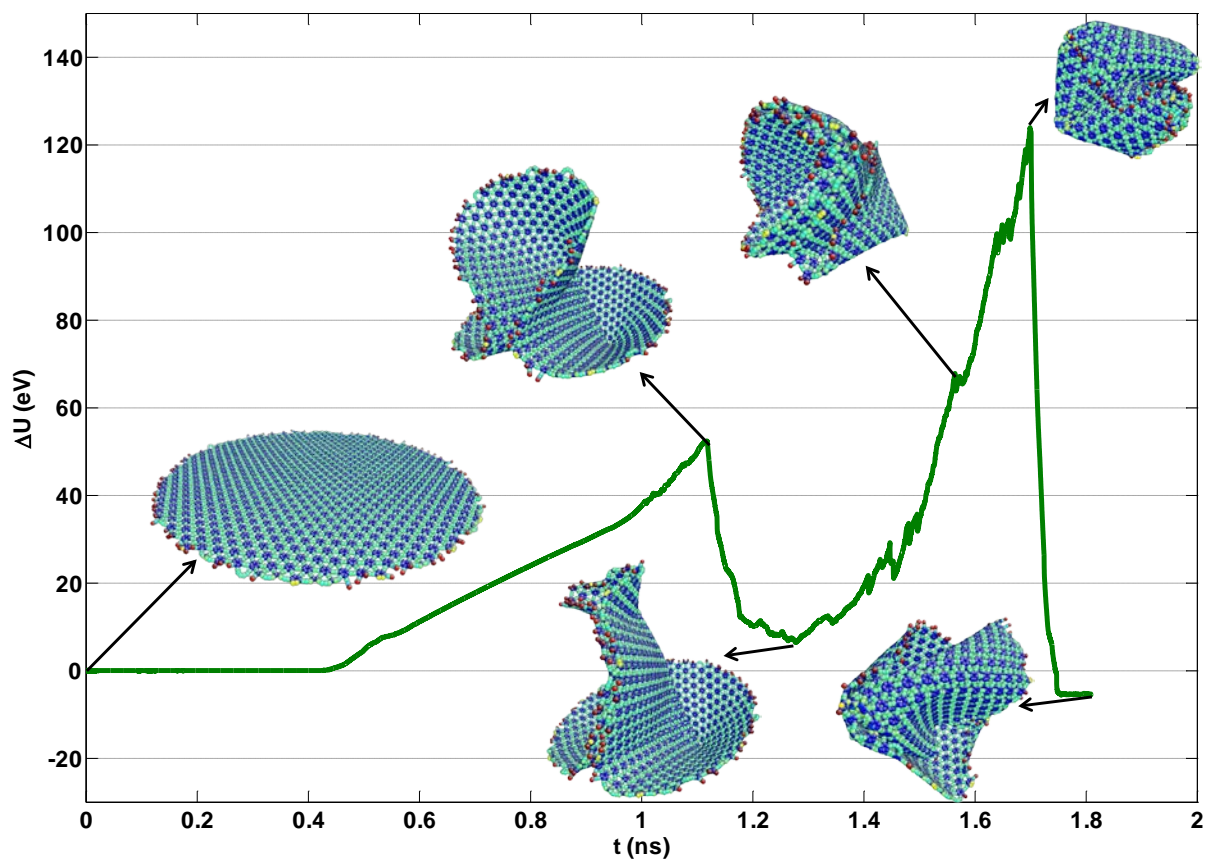


Figure 3: Potential energy of 1-graphyne undergoing crumpling as a function of time. Inserts show the crumpled graphyne at local minima and maxima. The crumpling rate is 5 nm/ns and the temperature is 1 K.

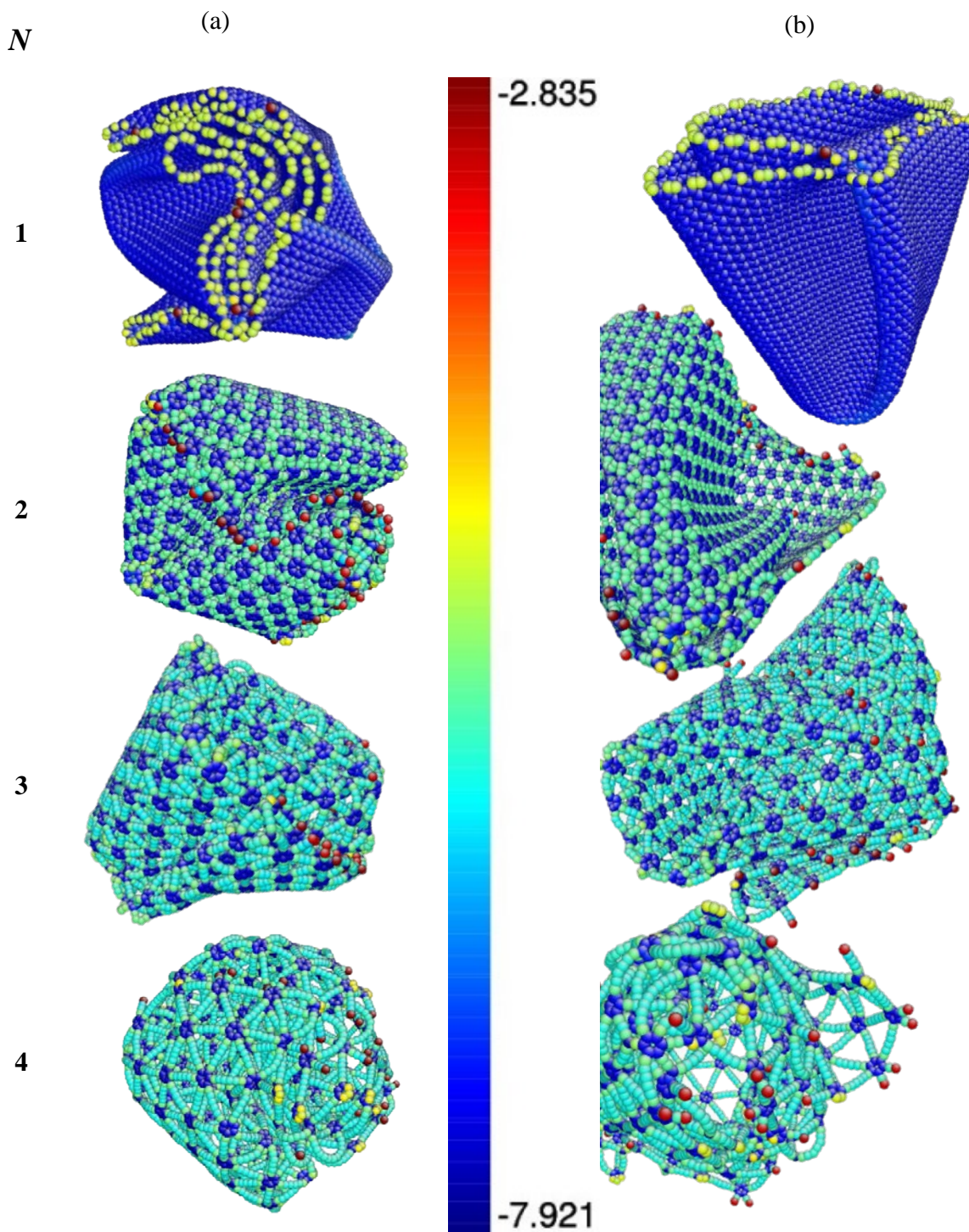


Figure 4: Potential energy maps of 10 nm circular crumpled *N*-graphyne (a) at maximum confinement and (b) after relaxation.

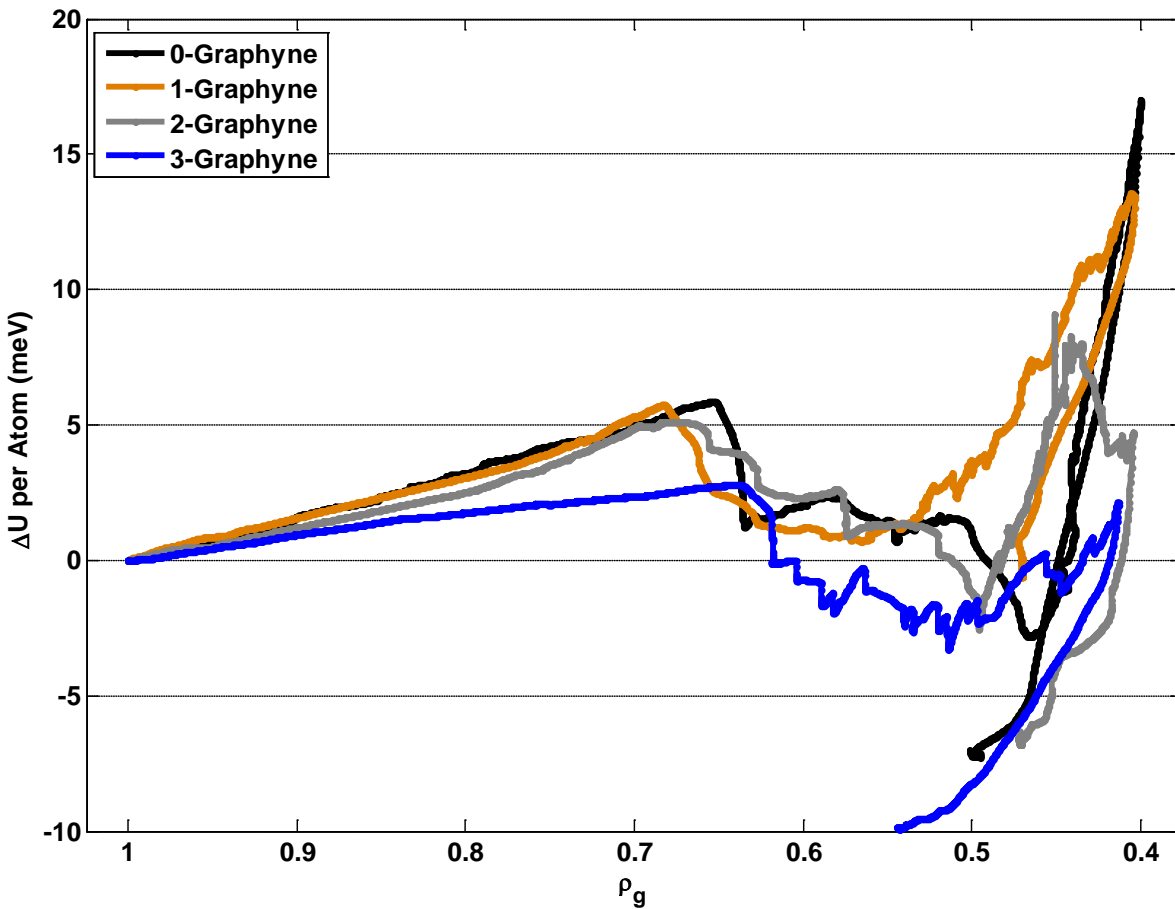


Figure 5: Change in U per atom as a function of the radius of gyration over the course of a run for N -graphynes. The crumpling rate is 5 nm/ns and the temperature is 1K.

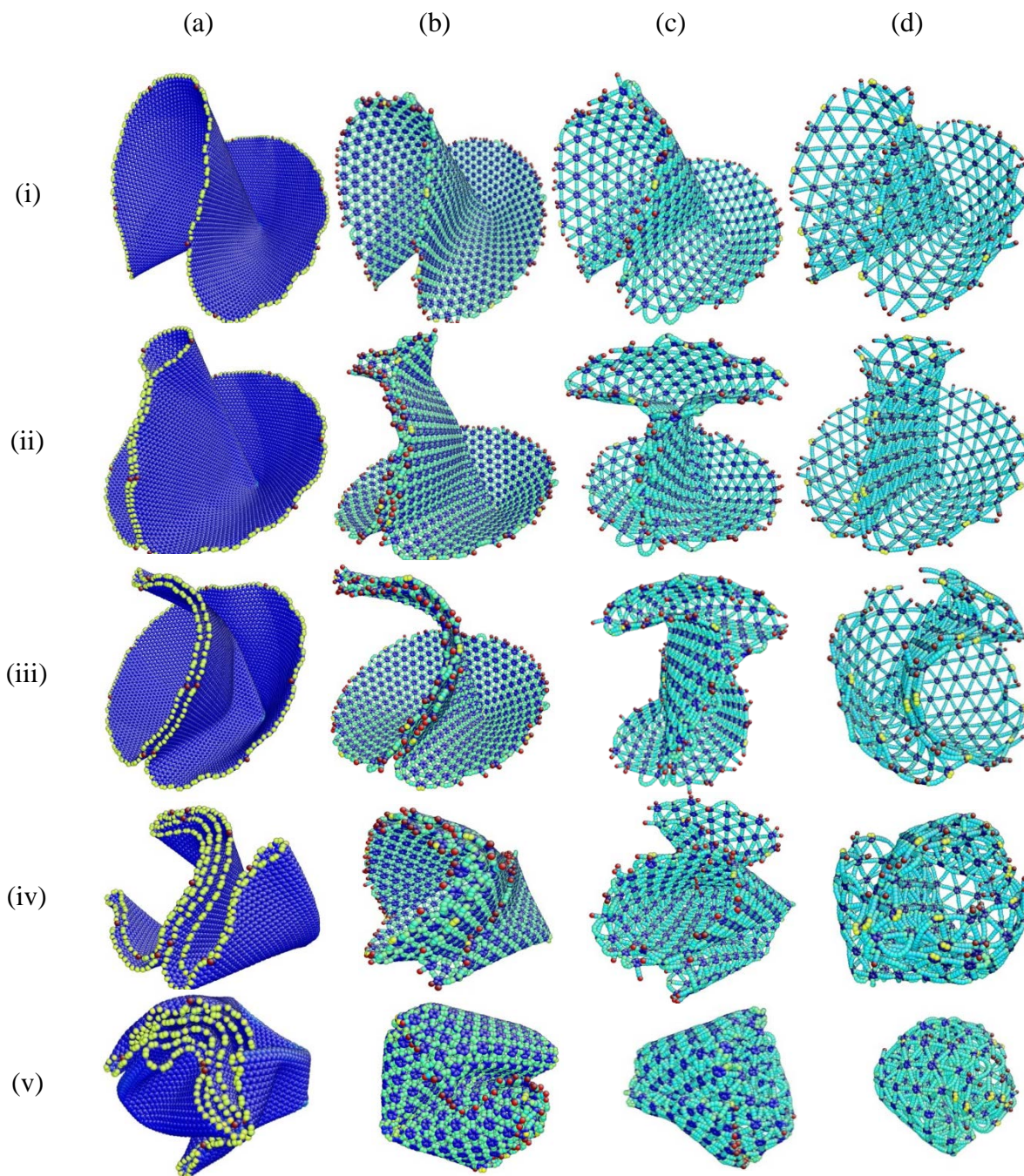


Figure 6: Comparison of circular N -graphynes during key stages (i-viii) of the crumpling process. Images from left to right are (a) 0-graphyne, (b) 1-graphyne, (c) 2-graphyne, and (d) 3-graphyne respectively.

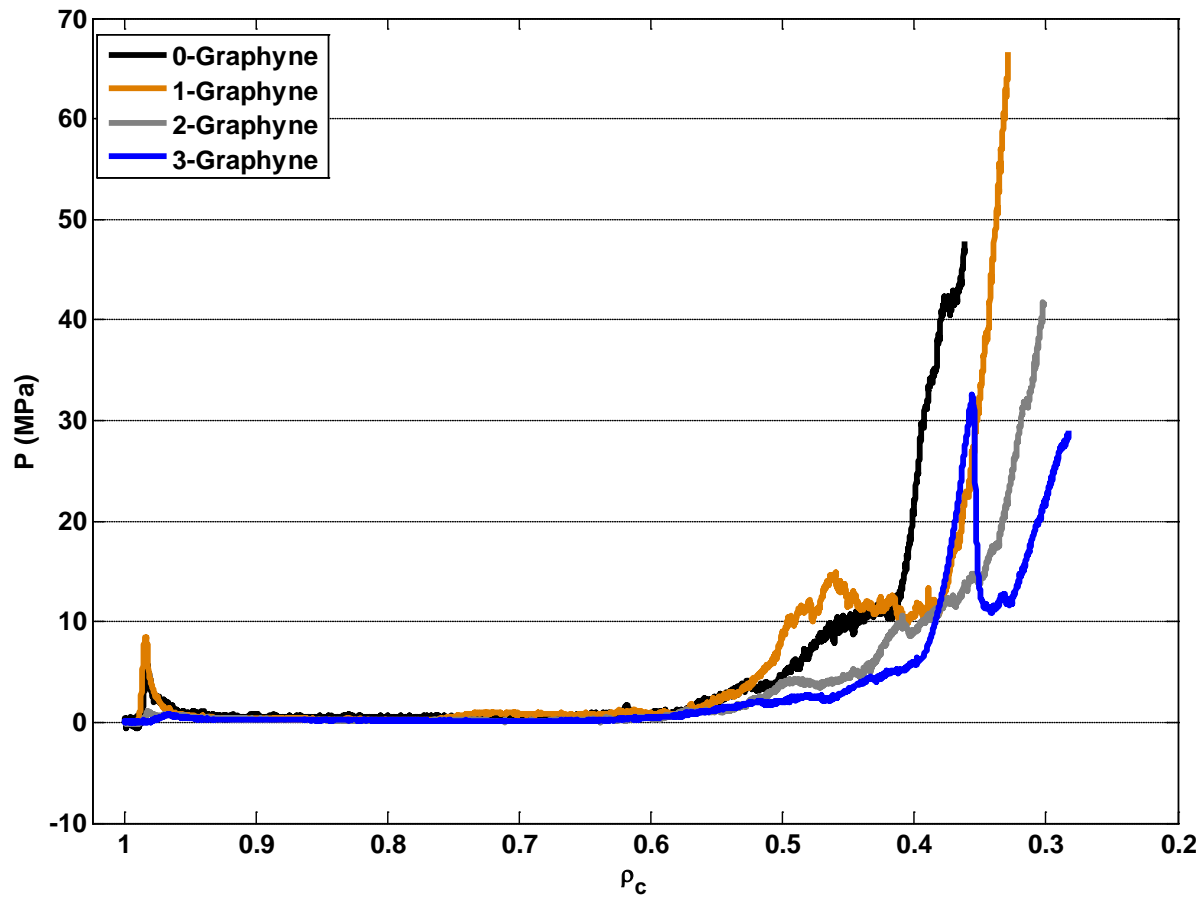


Figure 7: The pressure acting on the graphynes as the radius of confinement shrinks (heavy confinement).

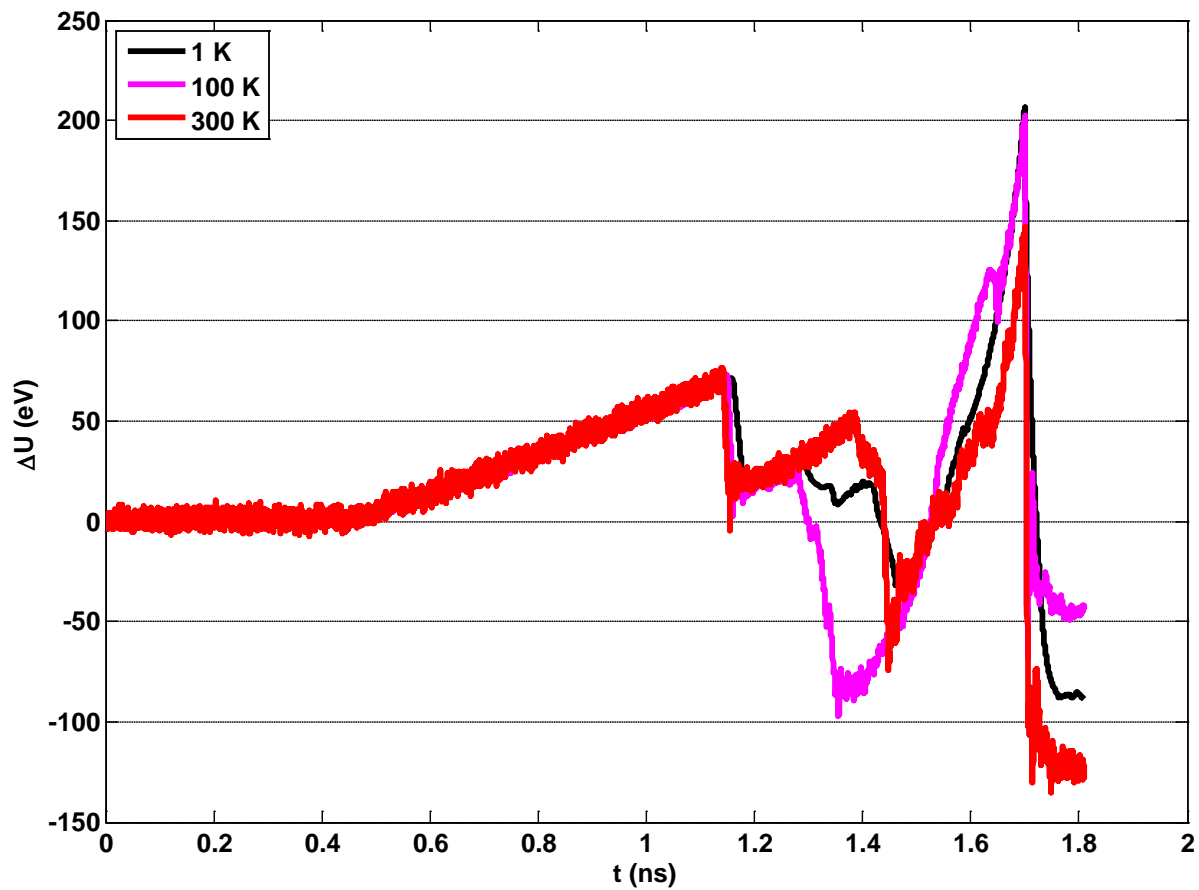


Figure 8: Change in potential energy versus time for 0-graphyne at different temperatures. Note the similarity in shape of the graphs, showing very similar behavior across several temperatures.

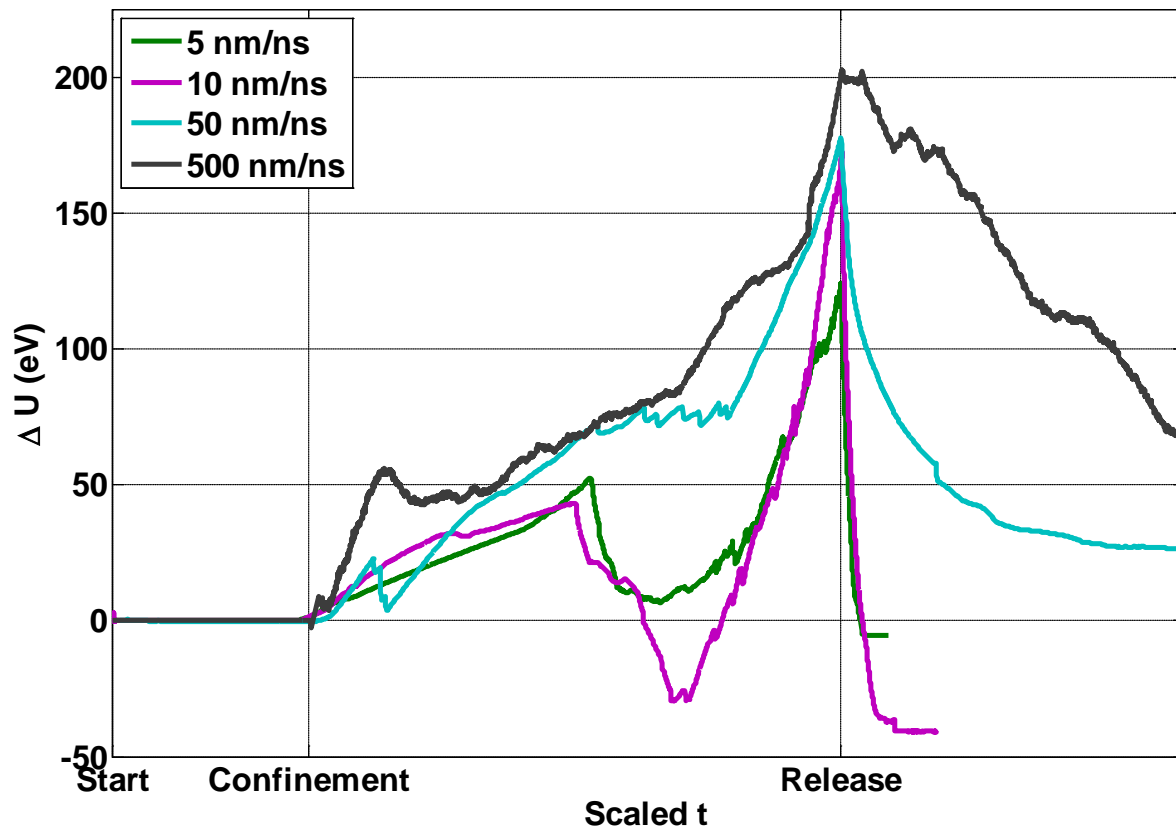


Figure 9: Change in U versus scaled time for 1-graphyne at 1 K undergoing different rates of confinement. The x -axis for each curve is scaled such that the confinement beginning and release are lined up. Note the similarity in shape of the graphs at low rates, and the increased U at higher crumpling rates.

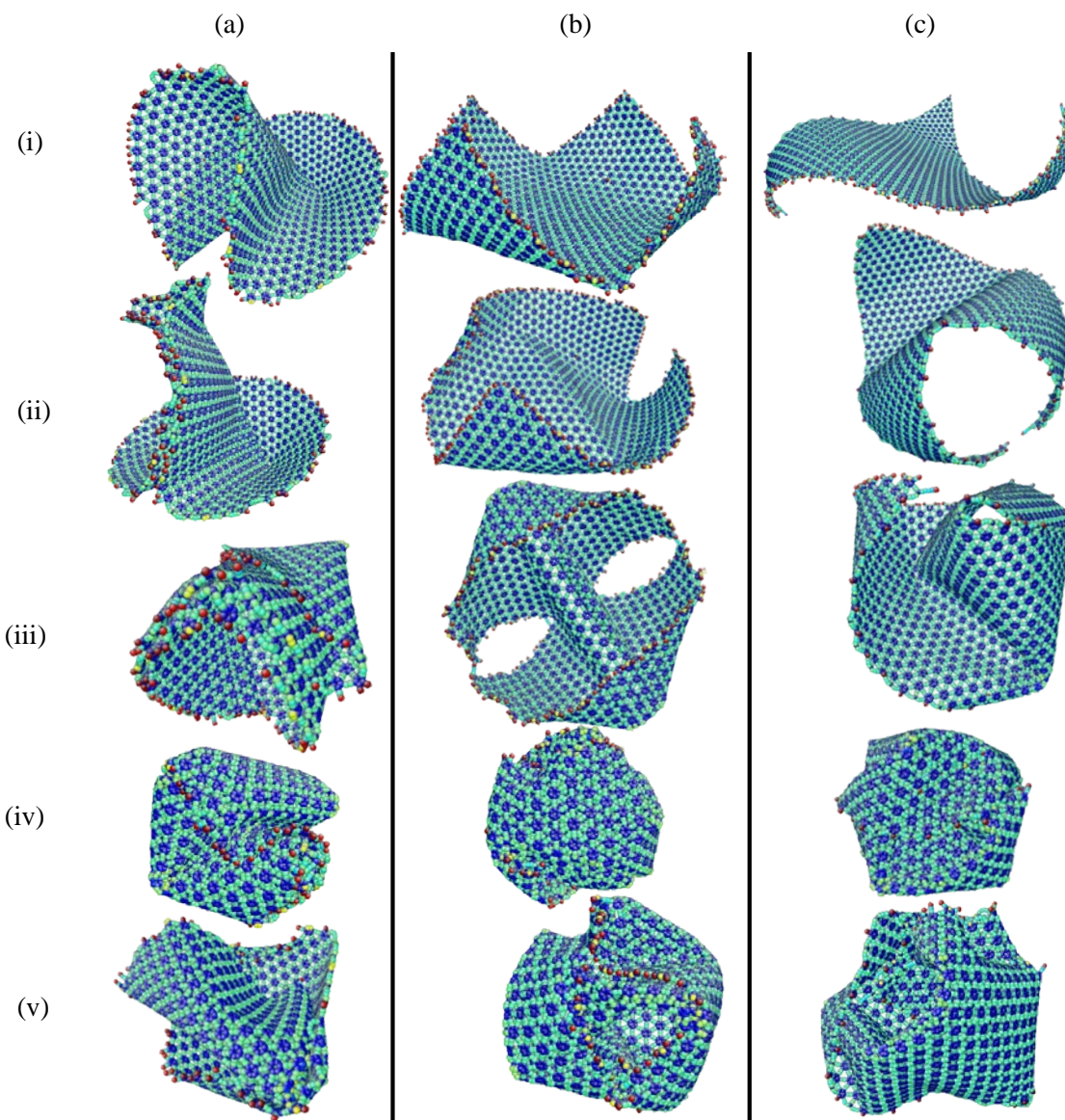


Figure 10: Nanosheets of 1-graphyne undergoing the crumpling process, column (a) is a circular nanosheet, column (b) has a square geometry, and column (c) is an equilateral triangle. All nanosheets have the same initial surface area. (i) - (iii) show the major crumpling stages, (iv) is the nanosheet under maximum confinement, and (v) is the equilibrated final structure.

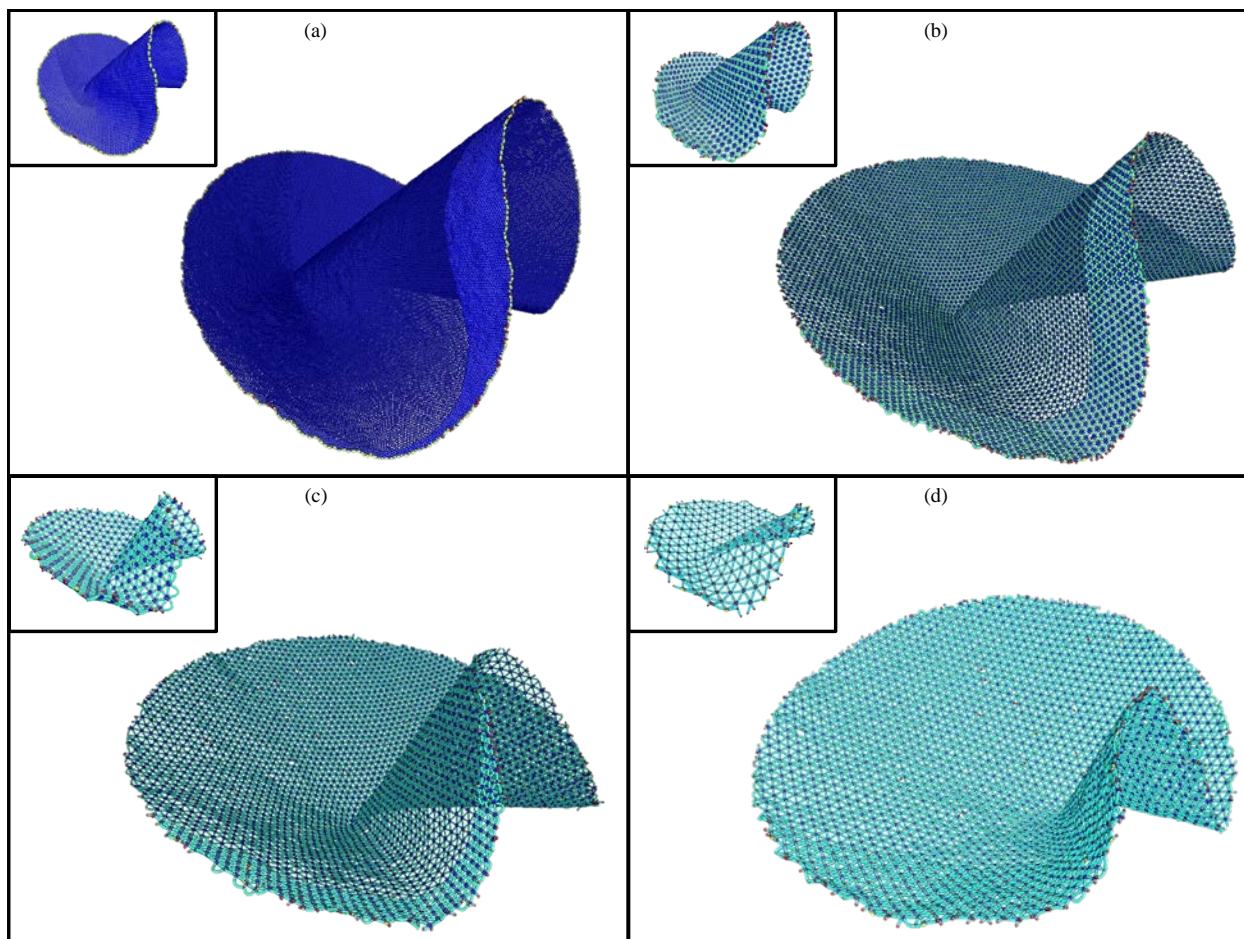


Figure 11: Large nanosheets of (a) 0-, (b) 1-, (c) 2- and (d) 3-graphyne showing the characteristic 'horn' shape during the initial stages of crumpling. The radius of the large nanosheets is 30 nm; images of the 10 nm radius nanosheets are inset for comparison.

Table 1: Overview of general properties of *N*-graphynes

<i>N</i>	Density relative to graphene	Hardness ²⁶ (MPa/nm)	Bulk Modulus ²⁶ (MPa)	Estimated Hardness (MPa/nm)	Estimated Bulk Modulus (MPa)
0	1.00	131	85	128.2	164.7
1	0.752	--	--	122.8	136.3
2	0.577	--	--	65.1	63.0
3	0.474	--	--	37.9	37.9